Relevance of Long Diffusion Lengths for Efficient Halide Perovskite Solar Cells

Samah Akel[●],[1,][*] Ashish Kulkarni[●],[1] Uwe Rau,[1] and Thomas Kirchartz[●][1,2,][†]

[1]*IEK5-Photovoltaik, Forschungszentrum Jülich, 52425 Jülich, Germany*

[2]*Faculty of Engineering and CENIDE, University of Duisburg-Essen, Carl-Benz-Str. 199,*
47057 Duisburg, Germany

Diffusion lengths are abundantly mentioned as a key enabler of high performance in lead-halide perovskite solar cells based on the implicit assumption that diffusion lengths are directly connected to efficient collection of charge carriers. While long diffusion lengths are indeed an important factor for highly efficient solar cells, they are a poor descriptor of efficient collection in the presence of undoped and low-mobility transport layers. Especially, the presence of low permittivity and organic electron- and hole-transport layers that are predominantly used in *p*-*i*-*n*-type perovskite solar cells can lead to substantial concentrations of electrons and holes within the perovskite absorber, as evidenced by measuring the photoluminescence at short circuit. These high carrier concentrations can lead to the seemingly odd situation in which charge collection at short circuit can be inefficient, even though the diffusion length substantially exceeds the absorber thickness. We use experiments, as well as analytical and numerical modeling, to define the requirements for both absorber and contact layers to enable efficient collection in perovskite solar cells.

I. INTRODUCTION

Long diffusion lengths are one of the most frequently stated attributes of lead-halide perovskites used for photovoltaics [1–3]. The appeal of the concept of a diffusion length is that it combines the two key electronic ingredients for efficient photovoltaics, namely, mobility, μ [4,5], and lifetime, τ [6–8], in one quantity with the intuitive dimension of a length [9–11]. Thus, long diffusion lengths are a convenient and usually implicit synonym for excellent electronic properties and efficient charge extraction [12,13]. The conventional textbook understanding of *p*-*n* junction solar cells predicts that charge collection is efficient if the (effective) diffusion length substantially exceeds the thickness of the device [9,14]. Hence, diffusion lengths of several micrometers in devices of typically only hundreds of nanometers thick are therefore a tempting argument for excellent charge collection. A key problem with this approach is, however, that the diffusion length,

as discussed in most textbooks [15,16], is strictly a concept describing the diffusion of *minority* carriers (e.g., electrons in a *p*-type semiconductor). In perovskite solar cells (PSCs), there is very little evidence for the absorber being strongly *p* type or *n* type given the intrinsic behavior [17,18], as generally seen in capacitance-voltage measurements [19]. At the same time, electric fields seem to be efficiently screened by the presence of moving ions [20–23]; this provides a strong argument that indeed diffusion (and not drift) is the relevant transport mechanism in the absorber. Hence, we might expect that a concept such as the ambipolar diffusion length that connects the properties of electrons and holes might be a good figure of merit for charge collection [24,25]. However, one remaining difference between many PSC designs [26–28] and that of most other photovoltaic technologies [29,30] is the presence of electron- and hole-transport layers, which often consist of poorly conductive low-permittivity organic semiconductors [31,32]. Charge-transport layers (CTLs) are designed such that they block one type of charge carrier and let the other pass [33–35]. This selectivity is achieved by an appropriate choice of electron affinity and ionization potential, thereby implementing blocking band offsets for minority carriers [36,37]. Thus, there are basically no minority carriers inside the CTLs, and hence, no recombination can happen within the layers [38,39]. Nevertheless, the CTLs are crucial to understand recombination in the absorber layer (the perovskite) [40] because they can have

[*]s.akel@fz-juelich.de

[†]t.kirchartz@fz-juelich.de

a huge effect on the steady-state concentrations of electrons and holes [41–43]. This modulation of the carrier concentration in the perovskite is an additional effect not captured by any textbook explanation of charge collection in solar cells. It can cause recombination losses at short circuit and low forward bias, even if the ambipolar diffusion length is much higher than the absorber thickness.

Here, we use a combination of numerical simulations and analytical equations to identify the requirements for efficient charge collection in widely used triple-cation lead-halide PSCs. We identify three ingredients for efficient charge collection, namely, a good diffusion length of the bulk, a low surface recombination activity, and a low resistance of the charge-transport layers. The relative importance of the three ingredients is controlled by the electrostatics of the device, i.e., the question of how the electrostatic potential difference provided by the contacts drops over the charge-transport layers and the perovskite absorber layer. We show that, given the excellent bulk lifetimes reported previously on lead-halide perovskites, the diffusion length is unlikely to limit charge collection in most high-quality perovskites. However, even if thin layers of a few tens of nanometers of low-mobility organic semiconductors are employed as the electron-transport layer (ETL) or hole-transport layer (HTL), substantial charge recombination at short circuit and low forward bias is likely and may affect the short-circuit current density, J_{SC}, without necessarily leading to a poor fill factor (FF). Furthermore, substantial recombination losses can appear, even if the bulk diffusion length exceeds the absorber thickness by several orders of magnitude, and are completely consistent with high open-circuit voltages (V_{OC}), relative to the band gap, that are observed in many halide perovskites [44,45].

II. THEORETICAL BACKGROUND

A. Charge collection in a *p-n* junction solar cell

The reason why the ratio of the diffusion length to the absorber layer thickness is considered a good figure of merit for charge collection in photovoltaics in general originates from the device physics of asymmetric *p-n* junctions, i.e., the type of junction most relevant for photovoltaic research for decades [46–48] In any *p-n* junction solar cell, a fairly large percentage of the volume is taken up by a doped region (*n* type or *p* type, the region is called the base), while only a tiny fraction of the volume is taken up by the space-charge region (SCR) and the oppositely doped region (called the emitter) [49,50]. In silicon photovoltaics, for instance, wafer thicknesses are typically on the order of 200 μm, while the width of the SCR and highly doped regions are in the hundreds of nanometer range. Modern silicon solar cells often use heterojunction designs [51–54] to move the oppositely doped regions out

of the actual wafer region to minimize Auger recombination losses in highly doped Si regions. In this situation of an asymmetric *p-n* junction, collecting minority carriers from the large neutral base region is a matter of diffusion rather than drift, given that the electric field is negligibly low outside of the small SCR. To mathematically understand charge collection of minority carriers in the (e.g., *p* type) base of a *p-n* junction, one would therefore have to solve the diffusion equation:

$$-D_n \frac{d^2 \Delta n}{dx^2} + \frac{\Delta n}{\tau} = G, \qquad (1)$$

where $D_n = \mu_n kT/q$ is the diffusion constant of electrons, Δn is the excess carrier concentration, τ is the lifetime of minority carriers, and G is the generation rate of free charges in the absorber (in the dark, $G = 0$). Here, μ_n is the mobility of minority carriers and kT/q is the thermal voltage. At short circuit, the boundary conditions [55] at the edge of the SCR ($x = 0$) and at the back contact ($x = d$) are typically assumed to be

$$\Delta n|_{x=0} = 0, \qquad (2)$$

and

$$\frac{J_n}{q} = -D_n \frac{d}{dx} \Delta n|_{x=d} = S_n \Delta n(d), \qquad (3)$$

where S_n is the surface recombination velocity. Note that, in particular, the validity and applicability of the first boundary condition [see Eq. (2)] are highly questionable. This assumes that at the edge of the SCR zero excess electrons are present under illumination. No matter how thin the emitter and SCR will be, charge transport through these layers will never be infinitely fast. Hence, under illumination, a finite excess carrier density will always be present in the SCR. Thus, the assumption $\Delta n|_{x=0} = 0$ is never met in reality, but it is often met well enough to make this theoretical approach useful. Later, when discussing PSCs, we come back to this type of boundary condition, because it is critical for understanding the relevance of the concept of a diffusion length for perovskite photovoltaics with low-conductivity contact layers. Finding a general solution for Eq. (1) with the two boundary conditions [Eqs. (2) and (3)] requires an explicit expression for the generation rate as a function of position x and is therefore often inconvenient or leads to rather lengthy equations [46]. To get an expression that is independent of the optics of the system but still captures the physics related to the electronic properties, it is therefore useful to define a collection efficiency of minority carriers. Using the Donolato relation [56–58], we obtain the collection efficiency of minority carriers $f_c(x)$, which is valid for the case of a recombination rate that is linearly proportional to the density of minority carriers and
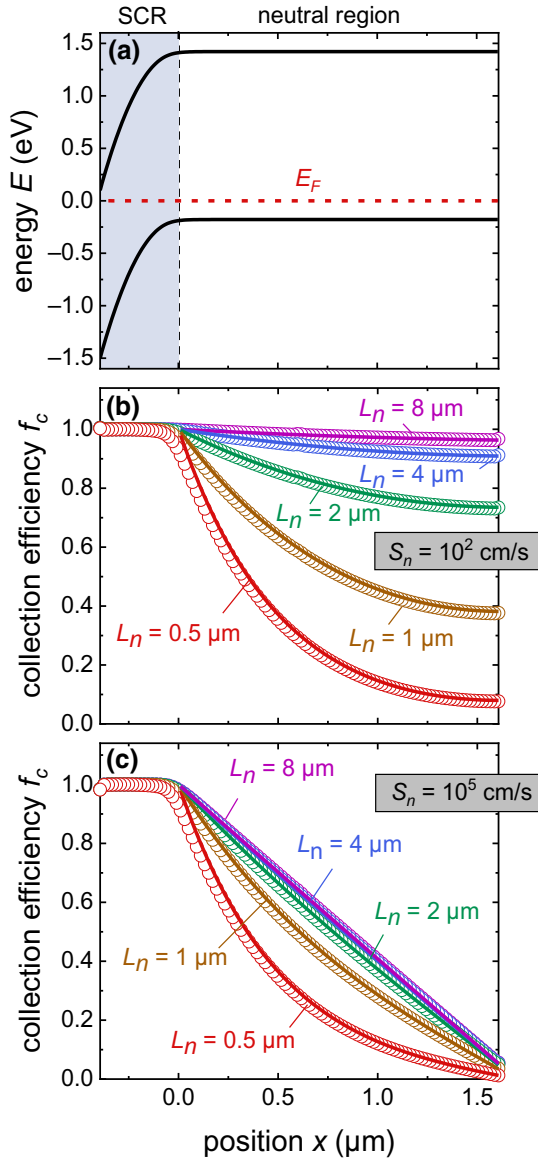
FIG. 1. (a) Energy-band diagram of an asymmetric p-n junction of a $2\,\mu$m-thick semiconductor with a p-type base of an acceptor density ($N_A = 10^{16}$ cm^{-3}), a carrier mobility ($\mu_n = \mu_p = 35$ cm^2/Vs), and a surface recombination velocity ($S_n = 10^2$ cm/s) under illumination and short circuit-conditions. (b) Collection efficiency of excess minority carriers (electrons) obtained using Eq. (4) (solid lines) by taking the boundary condition at the edge of the SCR as $n(0) = 0$, and their respective numerical simulation (open circles) for different diffusion lengths and a good surface of a recombination velocity of 10^2 cm/s . (c) Numerical (open circles) and analytical (solid lines) calculation of the collection efficiency of minority carriers (electrons) for different diffusion paths and for a bad surface ($S_n = 10^5$ cm/s).

defined as

$$f_c(x) = \frac{\Delta n(x)}{\Delta n(0)} = \cosh\left(\frac{x}{L_n}\right) - \frac{L_n}{L_{\text{eff}}} \sinh\left(\frac{x}{L_n}\right), \quad (4)$$

where L_n is the minority-carrier diffusion length, and L_{eff} is the effective diffusion length given by

$$L_{\text{eff}} = L_n \frac{(D_n/L_n)\cosh(d/L_n) + S_n \sinh(d/L_n)}{(D_n/L_n)\sinh(d/L_n) + S_n \cosh(d/L_n)}. \quad (5)$$

The effective diffusion length depends on the diffusion length of minority carriers in the absorber, L_n, and it is strongly affected by the quality of the surfaces via the surface recombination velocity, S_n, in Eq. (5).

To see how the diffusion length and the quality of the surfaces affect the collection of charge carriers that are generated in p-n junction solar cells, first we simulate the band diagram of a p-type semiconductor of a SCR of typically hundreds of nanometers (400 nm) and a neutral region (p type) of several micrometers (1.6 μm) at short circuit and under illumination, as shown in Fig. 1(a) We evaluate the collection efficiency of minority carriers (electrons), $f_c(x)$, analytically using Eq. (4) and numerically using a drift-diffusion simulation program called ASA [59] for different diffusion lengths and for two surfaces of different recombination activity. We consider a good surface to have a low recombination velocity of 10^2 cm/s and a bad one to have a high recombination activity ($S_n = 10^5$ cm/s). In Figs. 1(b) and 1(c), perfect collection implies $f_c = 1$, while the worst case would be complete recombination of the generated minority carriers with $f_c = 0$. For the situation of a good back surface, we observe an exponential decay of the collection efficiency of electrons that possess diffusion lengths smaller or, more likely, similar to the thickness of the p-type base, see Fig. 1(b) On the other hand, photogenerated electrons are only extracted very well if the diffusion length is several times longer than the thickness of the neutral region. In contrast, the really poor quality surface limits the extraction of minority carriers, despite the diffusion length exceeding the device thickness; for instance, we lose 50% of the electrons that are generated in the middle of the neutral region just due to the high recombination velocity of the back surface, although generated electrons have a long diffusion length (8 μm), as shown in Fig. 1(c). We conclude that the extraction of charge carriers of a reasonable diffusion length is only efficient if the surface recombination velocity, S_n, is small; otherwise, free excess carriers recombine and more photocurrent is lost. In any case, collection is an asymmetric function (being high close to the electron contact and low close to the hole contact), the characteristic decay of which is described by reasonably simple Eq. (4) that depends on L_n and L_{eff}, which therefore implies that the concept of a diffusion length (in combination with a surface recombination velocity) describes charge collection in a meaningful way.

B. Collection efficiency of photogenerated charge carriers in perovskite solar cells

1. State-of-the-art perovskite solar cells and the ambipolar diffusion length

We now leave behind the world of *p-n* junction solar cells and discuss how far the concept of a diffusion length is still meaningful in the context of lead-halide perovskite solar cells. Lead-halide perovskites have ideal properties for use in efficient solar cells. They have high absorption coefficients [60,61] and extremely long charge-carrier lifetimes [7,62] if compared within the class of direct semiconductors. Perovskite absorbers can be built as single crystals or thin films [63–66], and to transform them into PSCs, suitable contact layers have to be identified that allow the efficient injection and extraction of majority carriers while blocking the minority carrier [34,67] and reducing the amount of interface recombination [68–70]. In recent years, different architectures of PSCs have been developed, including the *p-i-n* structure, where an intrinsic perovskite material is sandwiched between a HTL (*p* type) and an ETL (*n* type) at the anode and the cathode, respectively [71]. To characterize the steady-state transport properties of electrons and holes in a PSC of an intrinsic absorber, we use the concept of the ambipolar diffusion length:

$$L_{\mathrm{amb}} = \sqrt{\frac{\mu k T}{q}(\tau_n + \tau_p)}, \qquad (6)$$

to act as an appropriate connection of the bulk lifetimes, τ_n and τ_p, for electrons and holes, and their mobility, μ. The interpretation of how efficient the PSCs are based on the efficient extraction of majority carriers requires two factors that substantially affect the amount of collected charges to be highlighted. The first is the diffusion length through the product of the lifetime and the mobility of free charge carriers [72], and the second is the kinetic properties or selectivity of the contacts [32,34,73]. Before discussing the effect of charge-carrier mobilities in contact layers on the collection of charge carriers in PSCs, we want to obtain a rough idea of what range of ambipolar diffusion lengths charge carriers possess in PSCs by looking at the lifetime and mobility values in the literature [74,75]. Typical lifetime values ranging between 0.1 and 10 µs are reported for perovskite thin films and similar values are recorded for single-crystal PSCs [76]. The mobility values for charge carriers in perovskite films and single crystals are mostly reported in the range between 1 and 100 cm²/Vs [4], whereby single crystals are more likely to be in the upper part of the range than thin films. Figure 2(a) shows a collection of lifetime values reported in the literature for thin films and single-crystal-based devices plotted as a function of thickness. To find out the typical range of ambipolar diffusion lengths for electrons and holes in
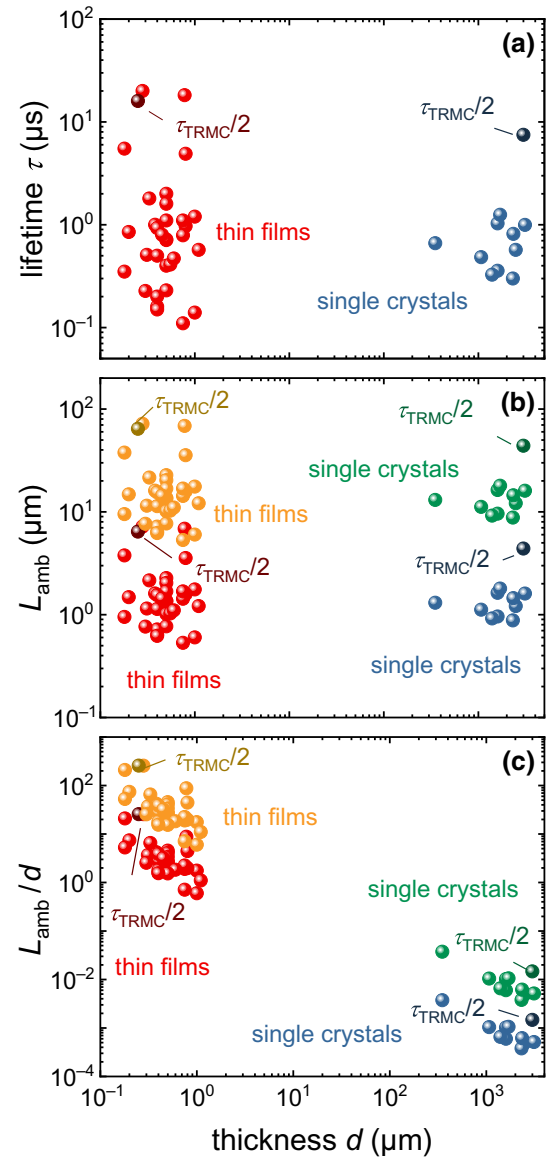

FIG. 2.   (a) Lifetime of free charge carriers based on the literature are obtained from the transient photoluminescence (TRPL) and transient microwave photoconductivity (TRMC) measurements on perovskite thin films and single crystals of different thicknesses (red and blue symbols, respectively). (b) Ambipolar diffusion length versus thickness of the perovskite calculated for the lifetime values shown in (a) for a low mobility of electrons and holes in the absorber ($\mu = 1$ cm²/Vs, red and blue spheres for thin films and single crystals, respectively), and for a high mobility of 100 cm²/Vs in the perovskite (the orange spheres for thin films and the green for single crystals). (c) Ratio of ambipolar diffusion length shown in (b) to the absorber thickness versus the thickness for thin films and single crystals. Panel (a) is reproduced and modified from Ref. [76]. Copyright the Authors of Ref. [72] (CC-BY license).

a perovskite absorber, we calculate L_{amb} using Eq. (6) for the lifetimes in Fig. 2(a) (for thin films and single crystals) and for charge-carrier mobilities of 1 cm²/Vs (red and

blue spheres) and 100 cm^2/Vs (orange and green spheres), as shown in Fig. 2(b). We choose these two mobilities as they represent approximately the higher and lower limits of the ranges of mobilities observed in meta-analyses of mobilities in lead-halide perovskites [4] (see simulations based on parameters from the literature in the Supplemental Material [77]). We obtain ambipolar diffusion lengths in the range of a few micrometers or slightly below for the case where $\mu = 1$ cm^2/Vs, while, in the more optimistic case, L_{amb} values go up to tens of micrometers. Figure 2(c) shows the diffusion lengths from Fig. 2(b) divided by the respective perovskite thicknesses. Here, the thin films cover a range of slightly below 1 to 100, while the single crystals are in the 10^{-2} to 10^{-3} range due to their millimeter thicknesses. Given that many of the lifetime values in the lower range may be affected by surface or interface recombination, it is likely that the diffusion length is frequently high enough to enable efficient collection in the logic of a traditional p-n junction. We investigate in the next section whether this is still true when taking the specific properties of the perovskite device geometries into account.

2. Charge transport and the extraction of the photocurrent in perovskite solar cells

Photogenerated charge carriers in PSCs are capable of successfully migrating a perovskite absorber of roughly 500 nm in the absence of electric fields without recombining. To understand how the diffusion and extraction of free charges take place in PSCs, we follow the general idea of Sandberg *et al.* [78], who deal with a perfectly symmetric device such that $n = p$ in the absorber layer. Furthermore, we assume the same kinetic properties of excess carriers in both CTLs that we express using the parameter S_{CTL} with the unit of velocity. The parameter S_{CTL} describes how fast transport of electrons through the ETL and holes through the HTL is. The transport equation of photogenerated charges (e.g., excess electrons, Δn) of an ambipolar diffusion length, L_{amb}, in an intrinsic perovskite material of a neutral zone (flat band) and under illumination conditions is defined as

$$-\frac{L_{\mathrm{amb}}^2}{(\tau_n + \tau_p)}\frac{d^2\Delta n}{dx^2} + \frac{\Delta n}{(\tau_n + \tau_p)} = G. \quad (7)$$

Here, we use an approximation for field screening by ions [22,23] by assuming an infinite permittivity ($\varepsilon \to \infty, F = 0$) in the perovskite. Solving this diffusion equation, in conjunction with the assumption of the perfect selectivity of contact layers [such that the ETL is perfectly selective for electrons, $J_p(d) = 0$, and the HTL allows only holes to diffuse through it, where $J_n(0) = 0$] results in the excess concentration of electrons and holes. The excess density,

Δn, in the absorber layer ($0 \le x \le d$) then follows from

$$\Delta n(x) = G(\tau_n + \tau_p)\left[1 - \cosh\left(\frac{x}{L_{\mathrm{amb}}}\right)C\right]. \quad (8)$$

By integrating the carrier density over the absorber thickness, we obtain their average concentration, Δn_{av}, as

$$\Delta n_{\mathrm{av}} = \frac{G(\tau_n + \tau_p)}{d}\left[d - L_{\mathrm{amb}}\sinh\left(\frac{d}{L_{\mathrm{amb}}}\right)C\right], \quad (9)$$

where C is a positive integration constant. Subsequently, the current density of excess electrons, J_n, inside the absorber follows as

$$J_n(x) = \mu kT\frac{d\Delta n}{dx} = -qL_{\mathrm{amb}}GC\sinh\left(\frac{x}{L_{\mathrm{amb}}}\right). \quad (10)$$

Likewise, an analogous procedure can be applied to obtain the density of excess holes, Δp, generated in the absorber and collected by the HTL. The current density of electrons flowing through the ETL can be determined as

$$J_n = -qS_{\mathrm{ETL}}\Delta n(x = d), \quad (11)$$

whereby S_{ETL} indicates how quickly excess electrons can move through the ETL to be collected at the cathode before they recombine. The hole current density in the HTL can be evaluated similarly, and thus, we write a general formula for the drift-diffusion velocity in the CTLs as

$$S_{\mathrm{CTL}} = \frac{\mu_{\mathrm{CTL}}U_{\mathrm{CTL}}/d_{\mathrm{CTL}}}{1 - e^{(-(U_{\mathrm{CTL}}/kT))}}. \quad (12)$$

In Eq. (12), μ_{CTL} is the mobility of electrons in the ETL and of holes in the HTL (both assumed to be equal). $U_{\mathrm{CTL}} = -Fd_{\mathrm{CTL}}$ is the potential difference across the CTLs, as shown in Fig. 3(a) for the potential difference across the ETL, and d_{CTL} is the CTL thickness (again both assumed to be equal). By using Eqs. (8), (10), and (11), we obtain an equation for the positive integration constant:

$$C = \frac{(\tau_n + \tau_p)S_{\mathrm{CTL}}}{L_{\mathrm{amb}}\sinh(d/L_{\mathrm{amb}}) + (\tau_n + \tau_p)S_{\mathrm{CTL}}\cosh(d/L_{\mathrm{amb}})}. \quad (13)$$

Finally, the collected photocurrent of electrons is obtained as

$$J_{\mathrm{SC}} = qGL_{\mathrm{amb}}\tanh\left(\frac{d}{L_{\mathrm{amb}}}\right)$$
$$\left[1 + \frac{\mu kT}{qL_{\mathrm{amb}}S_{\mathrm{CTL}}}\tanh\left(\frac{d}{L_{\mathrm{amb}}}\right)\right]^{-1}. \quad (14)$$
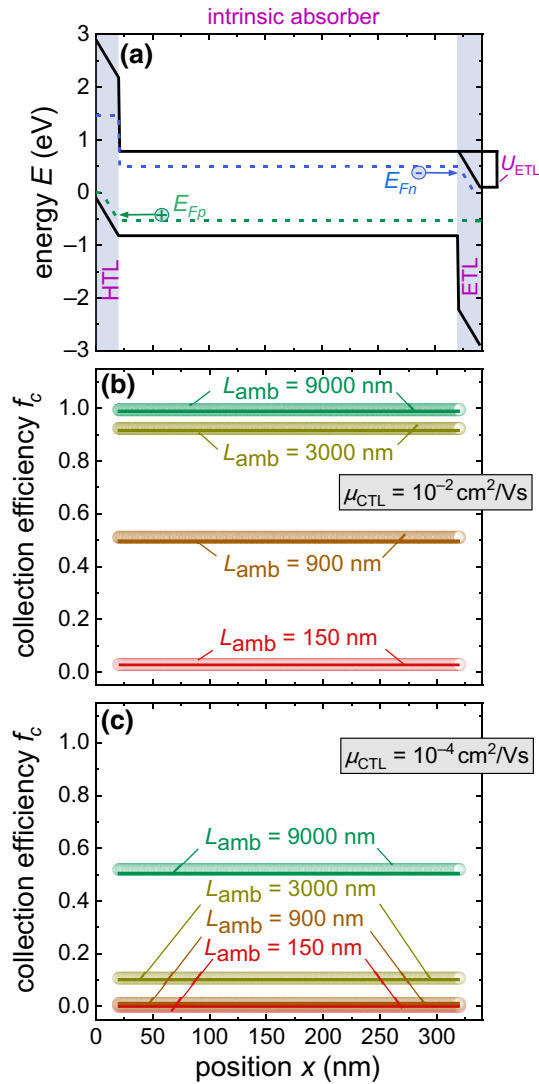
FIG. 3.   (a) Band diagram of a symmetric p-i-n junction of an intrinsic perovskite absorber ($\varepsilon_{\text{pero}} \to \infty$) of 300 nm sandwiched between a HTL and an ETL with $d_{\text{HTL/ETL}} = 20$ nm under illumination and short-circuit conditions. (b) Collection efficiency obtained by using Eq. (16) (solid lines), and their respective numerical simulation (open circles) for different ambipolar diffusion lengths and for good transport velocity in the CTLs with $\mu_{\text{CTLs}} = 10^{-2}$ cm²/Vs. (c) Numerical (open circles) and analytical (solid lines) evaluation of the collection efficiency for bad kinetic properties in the CTLs with $\mu_{\text{CTLs}} = 10^{-4}$ cm²/Vs. Highly resistive CTLs are significantly limiting the extraction of photogenerated charges at short circuit, despite possessing long ambipolar diffusion lengths.

To predict the extraction efficiency of excess charge carriers collected by the CTLs in a PSC, we start with

$$J_{\text{SC}} = q \int_0^d G(x) f_c(x) \, dx. \tag{15}$$

Equation (15) relates the obtained current density, J_{SC}, with the generation rate and the collection efficiency. By taking the ratio of the collected free carriers to those generated due to the absorption of light by the perovskite layer, we obtain their collection efficiency:

$$f_c = \frac{J_{\text{SC}}}{qGd}. \tag{16}$$

For a constant generation in the absorber, the extraction efficiency can be calculated via Eq. (16) through dividing the obtained short-circuit current density, J_{SC}, by the position-independent generation rate, G; the elementary charge, q; and the thickness of the perovskite, d.

To illustrate the impact of the ambipolar diffusion length and kinetic properties of the CTLs on the collection of charge carriers in PSCs, Fig. 3(a) presents the band diagram of a symmetric p-i-n junction of an intrinsic perovskite absorber (300 nm) sandwiched between two contact transport layers at short circuit and under illumination. We assume a flat band condition ($\varepsilon \to \infty$, $F = 0$) in the perovskite [23,79] (see the situation of including mobile ions in the Supplemental Material [77], Fig. S5). The band diagram is simulated for a mobility of 10^{-2} cm²/Vs in the CTLs and for an ambipolar diffusion length of 9000 nm. E_{Fn} and E_{Fp} are the Fermi levels of electrons and holes, respectively. The collection efficiency of charge carriers is simulated and analytically calculated for different ambipolar diffusion lengths and for good and bad transport properties in the CTLs, as shown in Figs. 3(b) and 3(c), respectively. The results show an efficient extraction of the photogenerated charge carriers possessing a long ambipolar diffusion length only if their mobility in the CTLs is good enough such that they are collected before undergoing any recombination mechanism; otherwise, more photocurrent losses will be present in the device. Therefore, the combination of reasonably high ambipolar diffusion lengths in the absorber and conductive CTLs is the requirement for efficient collection of photogenerated charges in PSCs.

III. RESULTS AND DISCUSSION

A. The effect of CTL mobility on excess carrier density for different ambipolar diffusion lengths in PSCs

The analytical framework described in Sec. II B eventually explains how the short-circuit current is reduced due to poor transport properties in either the absorber or contact layers. It is therefore useful to estimate the required mobilities in absorber and contact layers to ensure efficient charge collection in PSCs. Even perovskites with very long diffusion lengths can then still suffer from collection losses if the transport velocity in the ETL or HTL is too low. According to the traditional textbook theory of p-n junction solar cells, resistive losses mostly affect

the fill factor and reduce J_{SC} only in rare and extreme cases. Thus, Eq. (14) is at odds with this traditional understanding, as it predicts a reduced J_{SC} as a consequence of resistive transport layers. The difference between the framework in Sec. II B and the logic of a simple series resistance is that a low value of S_{ETL} or S_{HTL} increases the charge-carrier concentration in the perovskite absorber. Mathematically, the difference is that the properties of the ETL and HTL enter the boundary conditions for the solution of the diffusion equation and are not added to the series resistance in an equivalent circuit element. This modification of the boundary condition is not an aspect of exclusive relevance to perovskites; it is also relevant, for instance, for Si or $Cu(In, Ga)Se_2$ solar cells [55,80–84]. Furthermore, the approach is similar to the situation encountered in organic solar cells or thin-film silicon solar cells, where the transport resistance [85] or internal series resistance [86] of the absorber layer causes the Fermi-level splitting at short circuit to become significant. However, the present form, where the resistivity of the charge-transport layers has a significant influence on recombination at short circuit is of particular importance for perovskites. This is because perovskites are a rare example of materials with relatively high mobilities in the absorber and (often) lower mobilities and conductivities in the contact layers.

To study the effect of the contact layers on charge-carrier recombination at short circuit, it is illustrative to consider the carrier concentration in the case where the diffusion length is much longer than the absorber layer thickness ($d \ll L_{amb}$). To consider this matter, we return back to Eq. (8), which can be simplified for $d \ll L_{amb}$ to give

$$\Delta n(\mu_{CTL}) = G(\tau_n + \tau_p)\left(1 - \frac{S_{CTL}(\tau_n + \tau_p)}{d + S_{CTL}(\tau_n + \tau_p)}\right). \quad (17)$$

For the case where the absorber thickness is much greater than the length represented by the product of the drift-diffusion velocity in the CTL and the lifetimes in the perovskite ($d \gg S_{CTL}(\tau_n + \tau_p)$), the density of excess electrons (Δn) that remain in the absorber is expected to be high where $\Delta n = G(\tau_n + \tau_p)$, while if $S_{CTL}(\tau_n + \tau_p) \gg d$, a perfect extraction of the generated charges is predicted, where $C \rightarrow 1$, and thus, $\Delta n \sim 0$ (best situation corresponds to complete extraction). Once the carrier density at short circuit approaches the limit [$\Delta n = G(\tau_n + \tau_p)$] of poor extraction, there are as many charge carriers in the absorber at short circuit as there are at open circuit. Figure 4(a) illustrates this situation by presenting the carrier density calculated via Eq. (8) (solid lines) and numerically simulated using ASA (symbols) as a function of the CTL mobility at short circuit and using the bulk diffusion length as a parameter. For every value of diffusion length, the

excess carrier density is approaching the limit of no extraction [colored dashed lines in Fig. 4(a)] that corresponds to the open-circuit situation for sufficiently low values of CTL mobility. Figure 4(b) shows the recombination rate at
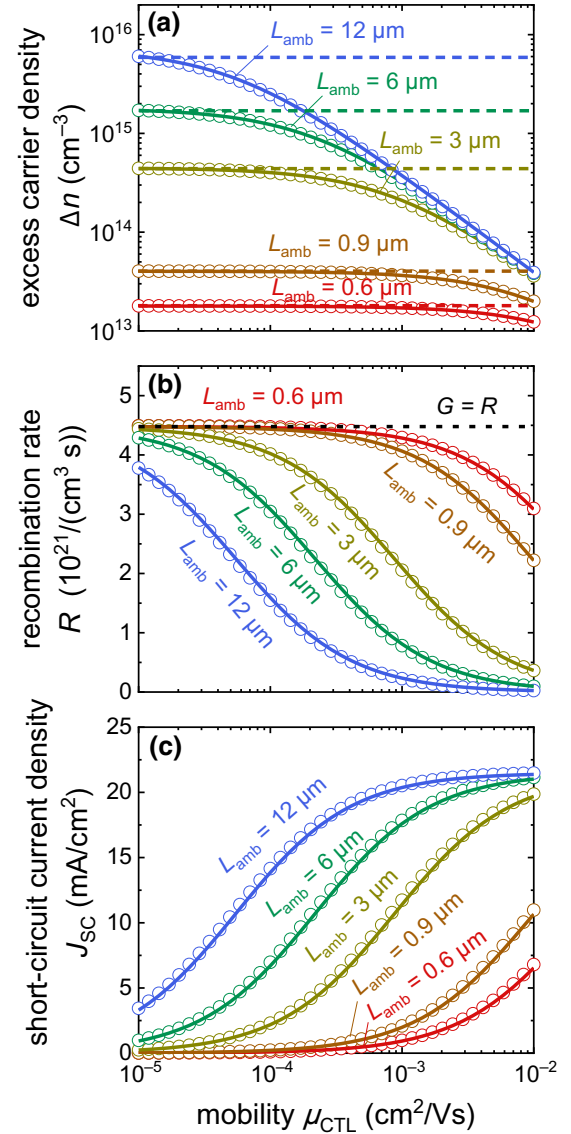

FIG. 4. Excess carrier density on the logarithmic scale as a function of charge mobility in the CTLs for different ambipolar diffusion lengths in the perovskite. Here, the perovskite mobility is kept constant at $\mu = 35$ cm^2/Vs, while the lifetime is changed. Simulated data are represented by open circles and the analytical calculation by solid lines. Dashed lines represent the saturated excess carrier concentration [$\Delta n = G(\tau_n + \tau_p)$] for different values of L_{amb}. (b) The Shockley-Read-Hall (SRH) recombination rate, R_{SRH}, of free charges in the absorber obtained by simulation and analytical evaluation (open circles and solid lines, respectively) compared to the generation rate for different L_{amb} and μ_{CTL}. (c) Simulated (symbols) and analytically calculated (solid lines) photocurrent as a function of mobility in the CTLs and with the ambipolar diffusion length as a parameter.

short circuit as a function of the kinetic properties in the CTLs and L_{amb} in comparison to the recombination rate at open circuit (dashed line). As the charge-carrier mobility in the CTLs increases, more charge carriers are extracted (less recombination) for a given L_{amb}. Given that at open circuit all photogenerated carriers recombine and none are extracted, it is clear that this situation is leading to zero photocurrent. While, at short-circuit charge carriers are extracted and take part in the obtained J_{SC}. Therefore, only if the carrier density at short circuit is substantially lower than the limit given by $\Delta n = G(\tau_n + \tau_p)$ is a considerable short-circuit current measured, as shown in Fig. 4(c). The key difference between the different situations is the CTL mobility that can still be tolerated to achieve a decent J_{SC}.

B. Quantifying photocurrent and efficiency losses due to μ_{CTL} in PSCs

In all simulations and analytical calculations presented so far, the ambipolar diffusion length is computed by changing the lifetime of charge carriers in the perovskite layer, whereas their mobility is kept constant. To see if any further improvements in the device performance can be achieved by changing the mobility in the absorber and not the lifetime, we simulate the photocurrent and cell efficiency; furthermore, J_{SC} is analytically calculated using Eq. (14) for different μ_{CTL} and different L_{amb}. For comparison, the ambipolar diffusion length is evaluated first by varying only the lifetime, τ, in the perovskite between 10^{-9} and 10^{-5} s, while the mobility is kept constant ($\mu = 35$ cm^2/Vs). In the other case, it is calculated by changing μ in the perovskite from 10^{-2} to 10^2 cm^2/Vs, while the lifetime is kept constant ($\tau = 10^{-6}$ s). In both approaches, we aim to obtain the same constant range of L_{amb}. The constant values of L_{amb} from both ways are increased up to more than 50 times of the absorber thickness, while the mobility of charge carriers in the CTLs is varied from a low mobility value of 10^{-5} cm^2/Vs to a high mobility of 10^{-2} cm^2/Vs. The obtained results for the first situation are shown in Figs. 5(a), 5(c), and 5(e), while those for L_{amb} with varied μ are shown in Figs. 5(b), 5(d), and 5(f).

Figure 5, with side-by-side panels, shows a disparate effect due to computing the ambipolar diffusion length by the two ways mentioned above on improving the obtained current density and cell efficiency at short circuit. In Figs. 5(a) and 5(b), it is clear that obtaining the same values of L_{amb} by the two approaches does not lead to the same photocurrent for any constant μ_{CTL}. For the situation where L_{amb} results from a varied lifetime and constant mobility in the bulk, the photocurrent seems to be improved for any given value of μ_{CTL} as L_{amb} increases. In contrast, increasing L_{amb} by changing the mobility in the perovskite and for any constant μ_{CTL} does not seem to be beneficial in improving J_{SC} and the device performance, especially

for the highly resistive CTLs. The simulated J_{SC} for both approaches can also be read from the 2D color plots represented in Figs. 5(c) and 5(d). The same influence on the cell efficiency by either varying the lifetime, Fig. 5(e), or the mobility, Fig. 5(f), in the perovskite with μ_{CTL} as a parameter is obtained by numerical simulation. Thus, once the absorber layer mobility is sufficiently high, any improvement in L_{amb} is only beneficial if it is an improvement in the electron and hole lifetimes, but not if it is an improvement in the mobility at a constant lifetime in the perovskite [72].

Figure 5(a) shows how J_{SC} is limited by the kinetic properties in the CTLs, even if L_{amb} is several times longer than the absorber thickness (at the highest shown $L_{amb} = 16$ μm, the ratio $L_{amb}/d \approx 53$). For a certain mobility value in the CTLs, it is clear that, as L_{amb} increases, the collected J_{SC} and the simulated cell efficiency, Figs. 5(c) and 5(e), increase and start to saturate for longer ambipolar diffusion lengths. However, reducing the mobility in the CTLs by orders of magnitude significantly increases the losses in the extracted photocurrent and the cell efficiency, e.g., approximately 16 mA/cm^2 photocurrent and 21.6% efficiency are lost by decreasing the mobility in the CTLs by 3 orders of magnitude. The results indicate how significantly the kinetic properties of charge carriers in the CTLs affect the collected photocurrent and the efficiency of functional PSCs, despite possessing long ambipolar diffusion lengths, and show their critical impact on reducing the device performance by slowing down the extraction of free electrons and holes ending with high losses.

C. Using band diagrams to visualize collection losses

Band diagrams are routinely used to visualize the behavior of electronic devices. While the analytical model presented in Sec. II B does not by itself produce a band diagram, it is easily possible to simulate band diagrams with numerical simulation software, such as ASA. To visualize the effect that varying transport velocities in the contact layer have on current-voltage curves and band diagrams, we present a comparison in Fig. 6. Figure 6(a) shows simulated current density (J) versus voltage (V) curves of two perovskite solar cells that differ in the assumed mobility in the CTLs. From the simulated J-V curves, we observe that the low mobility in the CTLs limits J_{SC} and the FF, while V_{OC} remains almost constant. In addition to the J-V curves, the band diagrams are simulated under different bias conditions: at open circuit, Fig. 6(b); at short-circuit, Fig. 6(c); and at the maximum power point (MPP) of the green J-V curve, Fig. 6(d). For all situations, the quasi-Fermi levels of electrons (E_{Fn}) and holes (E_{Fp}) in the absorber are flat, because we assume an infinite permittivity to obtain a field-free absorber layer. The key differences between the high and low CTL mobilities in the band diagram are the gradients of E_{Fn} and E_{Fp} in the transport layers [32,79] for the situations where a current is flowing (i.e., at short
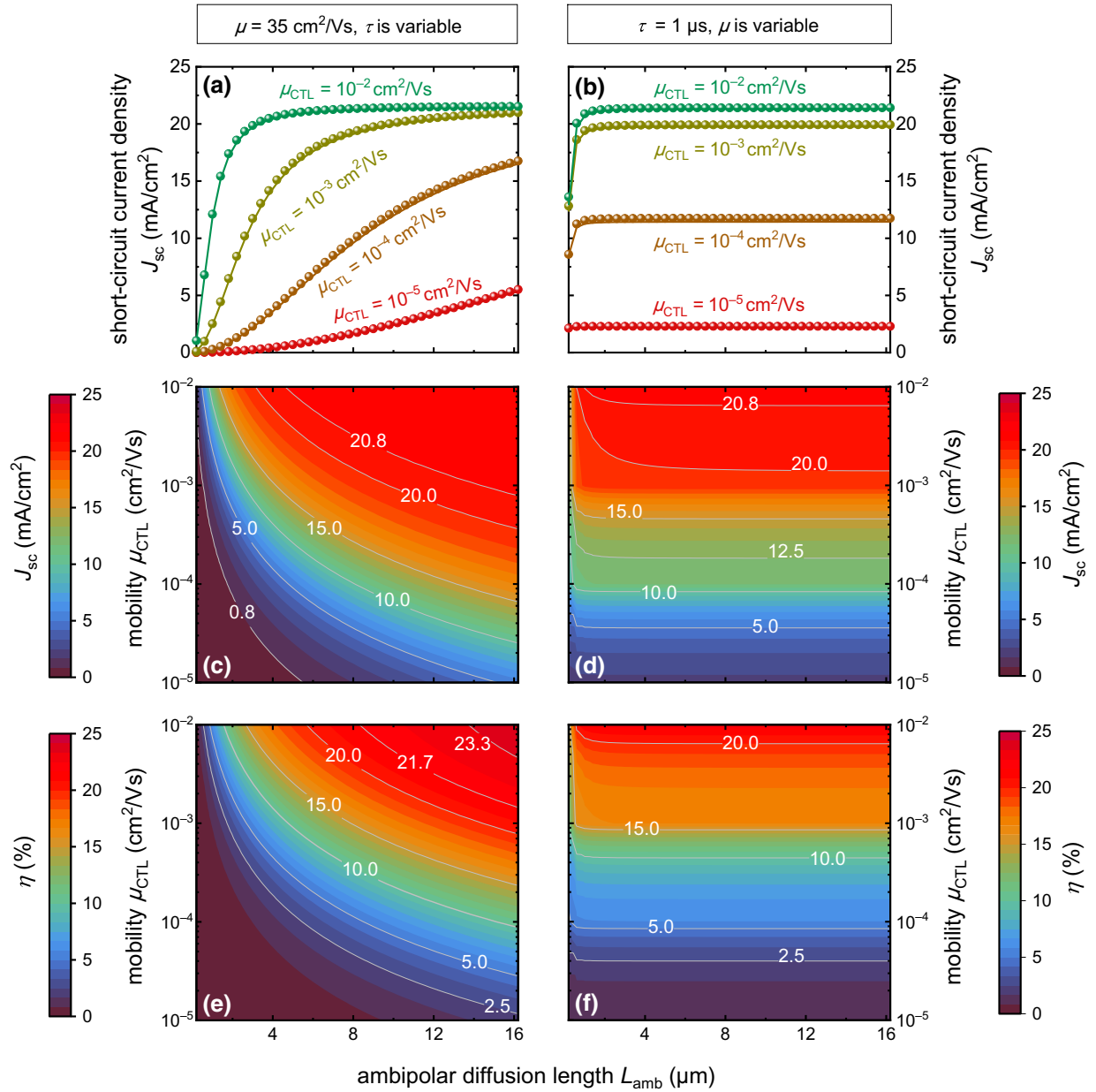
FIG. 5. Simulated and analytically calculated (symbols and solid lines, respectively) data of (a) short-circuit current density as a function of ambipolar diffusion length with a varied lifetime (10^{-9} to 10^{-5} s) and a constant mobility (35 cm^2/Vs) of charge carriers in a perovskite layer of 300 nm and for different mobilities in the CTLs. (b) Short-circuit current density, J_{SC}, is obtained for the same range of ambipolar diffusion lengths in (a) but with a constant lifetime of 10^{-6} s and a varied mobility in the bulk (10^{-2} to 10^2 cm^2/Vs); kinetic properties in the CTLs are also changed such that μ_{CTLs} goes from 10^{-5} to 10^{-2} cm^2/Vs in both (a),(b). (c),(d) Two-dimensional (2D) color plots of simulated J_{SC} correspond to (a),(b), respectively. (e),(f) Efficiency of a PSC obtained numerically by ASA for different ambipolar diffusion pathways [L_{amb} in panels (a),(b), respectively] and with CTL mobility as a parameter represented in 2D color plots.

circuit and at MPP). We know that the current densities for electrons and holes are given by $J_n = \mu_n n dE_{Fn}/dx$ and $J_p = \mu_p p dE_{Fp}/dx$. Thus, for a given current density, J_{SC}, to flow, the gradient of the quasi-Fermi level in the ETL has to follow $dE_{Fn}/dx = J_{SC}/(\mu_n n)$. Equivalently, in the HTL, the quasi-Fermi level for holes has to obey $dE_{Fp}/dx = J_{SC}/(\mu_p p)$, because in the ETL (HTL)

the current is purely an electron (hole) current. Thus, if the mobility in the CTLs is reduced, the gradient of the quasi-Fermi level has to increase, thereby leading to a higher splitting of the quasi-Fermi levels in the absorber. This increased splitting can be observed both at short circuit and at the MPP. Given that recombination increases with increasing carrier density, and therefore, with

increasing quasi-Fermi-level splitting, the increased gradients of E_{Fn} and E_{Fp} are directly responsible for the reduced performance of the curve with lower mobility, as seen in Fig. 6(a). The finding of Fig. 6 is therefore essentially identical to that of Fig. 4, but it also allows the physics of the analytical model to be illustrated within the logic of band diagrams.

IV. CHARGE-CARRIER COLLECTION AND PHOTOLUMINESCENCE

Measuring the photoluminescence (PL) emission of halide perovskite films, layer stacks, and solar cells is a widely used approach to quantify recombination losses and to study the amount by which recombination changes when adding additional interfaces that usually accelerate recombination [41,87,88]. However, even in the case of the PL of complete solar cells, the experiment is typically performed at open circuit, where no current is flowing through the external circuit. Thus, charge-carrier transport is nearly irrelevant, as we have already seen in the open-circuit band diagram in Fig. 6(b). Transport is however relevant either in transient PL experiments, where exchange currents are flowing from the absorber to the contact and back [65,89], or in steady-state PL experiments that are performed on complete solar cells at voltages below V_{OC} [90–92]. In the following, we take a closer look at PL measured as a function of voltage and, in particular, PL measured at short circuit and how it is related to the analytical framework presented in Sec. II B.

The PL emission from the perovskite is proportional to the product, np, of the electron and hole concentrations in the perovskite layer. If the perovskite is intrinsic, as we assume throughout the paper, the PL emission will be proportional to n^2 [40,41,93] (see Figs. S5 and S6 within the Supplemental Material [77]). At open circuit, the PL emission at a given excitation condition should be as high as possible—a fact that is frequently used in the context of suns-PL measurements [94] in various photovoltaic technologies. The Fermi-level splitting, ΔE_F, that can be reached is given by

$$\Delta E_F = kT\ln\left(\frac{np}{n_i^2}\right) = kT\ln(\Phi) + A, \quad (18)$$

where Φ in Eq. (18) is a dimensionless quantity in arbitrary units, and A is a typically unknown constant that accounts for the fact that photon flux is only typically known in relative units. Thus, any relative change in the PL intensity from sample to sample (assuming equal band gap and absorptivity) by a factor Φ would correspond to an additive change in ΔE_F by an amount $kT\ln(\Phi)$.

At open circuit, the average generation and recombination rates are equal and charge extraction is nonexistent by definition. At voltages $V_{ext} < V_{OC}$, however, charge is extracted, and the rate of recombination is then ideally much lower than the rate of generation. Thus, for a good solar cell, the carrier concentration away from open circuit should be as small as possible, whereby the lower limit under illumination is given by the carrier density injected from the contacts given by

$$np > n_i^2\exp\left(\frac{qV_{ext}}{kT}\right). \quad (19)$$

Ideally, a PSC with perfect extraction should therefore have no additional PL at $V_{ext} < V_{OC}$ that would exceed the open-circuit PL at a lower excitation intensity and the same voltage [95]. However, in practice, slow carrier extraction leads to quite substantial quasi-Fermi-level splitting [see Figs. 6(c) and 6(d)], and thus, carrier density and PL intensity. The PL at short circuit is then directly proportional to the square of the carrier density at short circuit that we derive with our analytical model [see, e.g., Eqs. (9) and (17)] and that is mainly a consequence of low carrier mobilities in the charge-transport layers. Thus, PL measurements at short circuit [96,97] or voltage-dependent photoluminescence [95] of complete PSCs are an ideal way to quantify the residual nonextracted carrier density present in the device and consequently the recombination losses present in the cell [98]. At high-level injection, we can use the following extremely simple relation:

$$\frac{\Delta n_{SC}}{\Delta n_{OC}} = \sqrt{\frac{\Phi_{SC}}{\Phi_{OC}}}, \quad (20)$$

to put the carrier density at short circuit in relation to the one at open circuit. By equating $qV_{OC} = \Delta E_F|_{OC}$, and from knowing the value of n_i^2, we can then at least provide an estimate of Δn_{SC} that can be compared with the results from Eqs. (9) and (17).

A. Correlating photoluminescence with device performance metrics

Given that the recombination current, $J_{rec}(V_{OC})$, at open circuit is identical to the maximum possible short-circuit current density, $J_{SC,max}$, in the absence of recombination, we can write

$$\frac{J_{SC}}{J_{SC,max}} = 1 - \frac{J_{rec}(0)}{J_{rec}(V_{oc})}. \quad (21)$$

If we combine the assumptions of high-level injection ($n=p$) and dominant SRH recombination, i.e., $J_{rec} \propto \Delta n/(\tau_n + \tau_p)$, we can write

$$\frac{J_{SC}}{J_{SC,max}} = 1 - \frac{\Delta n_{SC}}{\Delta n_{OC}} = 1 - \sqrt{\frac{\Phi_{SC}}{\Phi_{OC}}}. \quad (22)$$

Note that the above assumptions imply that the ideality factor of recombination is $n_{id} = 2$, which is sometimes
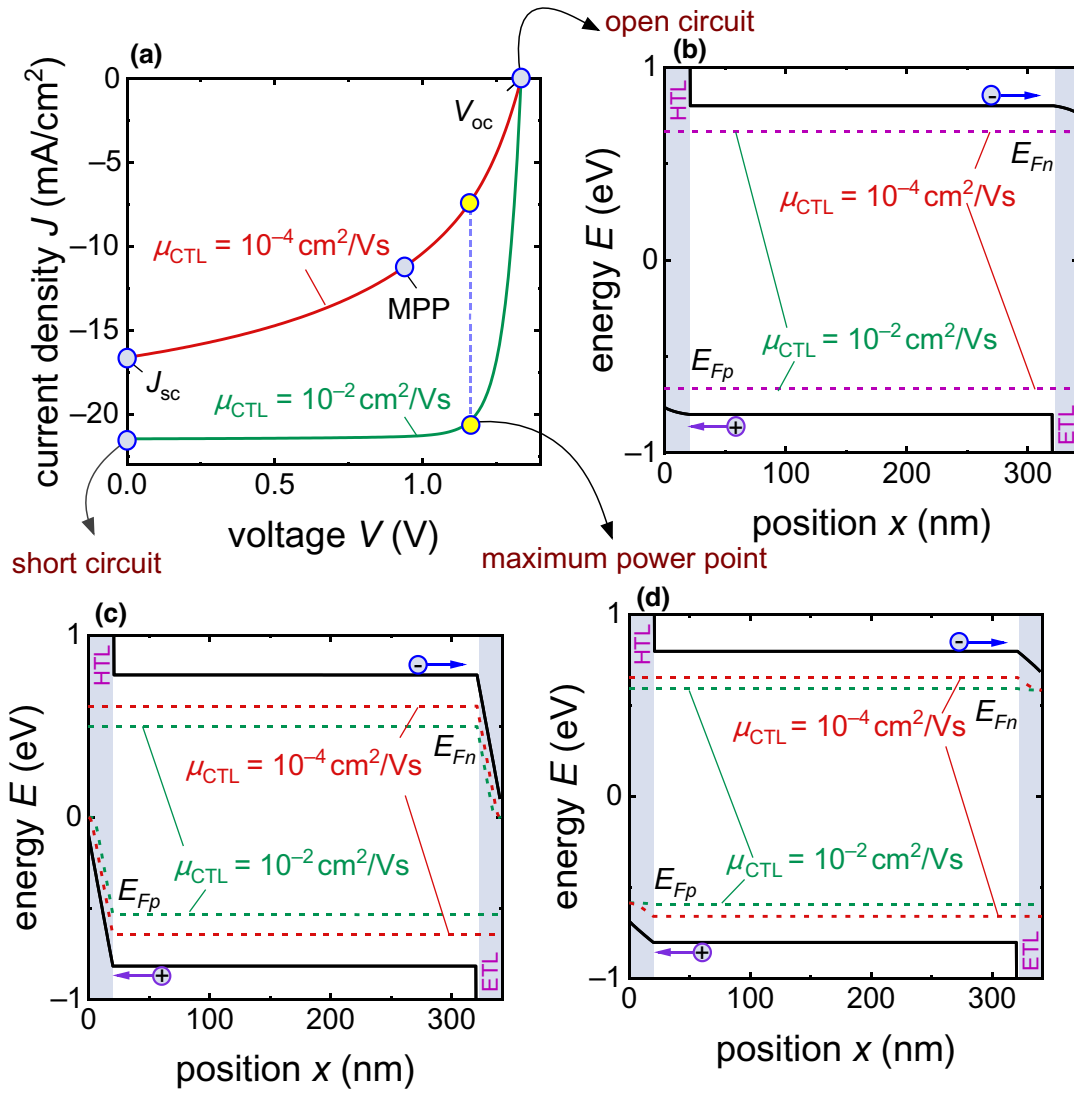
FIG. 6. (a) Simulated J-V curves of two solar cells with a layer stack representative for PSCs. Green J-V curve is for a cell with good transport properties of electrons and holes in the CTLs (where $\mu_{\mathrm{CTL}} = 10^{-2}\,\mathrm{cm^2/Vs}$), while the red curve is for a cell with poor mobility of free charge carriers in the CTLs. Band diagram of both devices is simulated at different bias conditions and under illumination with a constant generation rate in the absorber ($G = 4.48 \times 10^{21}\,\mathrm{cm^{-3}\,s^{-1}}$). Applied bias conditions are (b) $V_{\mathrm{ext}} = V_{\mathrm{OC}}$, (c) $V_{\mathrm{ext}} = 0\,V$, and (d) $V_{\mathrm{ext}} = V_{\mathrm{MPP}}$ [the maximum power point of the cell with better transport properties in the CTLs; yellow circles in (a)].

but not always a realistic case for halide perovskite solar cells [39,99–101]. In a more general case, where $J_{\mathrm{rec}} \propto \exp(\Delta E_{\mathrm{F}}/(n_{\mathrm{id}}kT))$, we find [84]

$$\frac{J_{\mathrm{SC}}}{J_{\mathrm{SC,max}}} = 1 - \left(\frac{\Phi_{\mathrm{SC}}}{\Phi_{\mathrm{OC}}}\right)^{(1/n_{\mathrm{id}})}. \tag{23}$$

For consistency with our analytical model, we continue using the special case given by Eq. (22). In this case, we can use Eq. (17) to express J_{SC} loss analytically. In the logic discussed above, $\Delta n_{\mathrm{OC}} = G(\tau_n + \tau_p)$, and hence, in

the limit $L_{\mathrm{amb}} \gg d$, we find

$$\frac{J_{\mathrm{SC}}}{J_{\mathrm{SC,max}}} = 1 - \frac{\Delta n_{\mathrm{SC}}}{\Delta n_{\mathrm{OC}}} = \frac{S_{\mathrm{CTL}}(\tau_n + \tau_p)}{d + S_{\mathrm{CTL}}(\tau_n + \tau_p)}. \tag{24}$$

If we do not impose a condition on L_{amb}, we obtain the following more general equation:

$$\frac{J_{\mathrm{SC}}}{J_{\mathrm{SC,max}}} = 1 - \frac{\Delta n_{\mathrm{SC}}}{\Delta n_{\mathrm{OC}}}, = \frac{L_{\mathrm{amb}}}{d}\sinh\left(\frac{d}{L_{\mathrm{amb}}}\right)$$
$$\frac{(\tau_n + \tau_p)S_{\mathrm{CTL}}}{L_{\mathrm{amb}}\sinh(d/L_{\mathrm{amb}}) + (\tau_n + \tau_p)S_{\mathrm{CTL}}\cosh(d/L_{\mathrm{amb}})}. \tag{25}$$

To see how the ratio of $\Delta n_{SC}/\Delta n_{OC}$ works in the logic of Eq. (25) and to understand what information this ratio gives, we calculate $\Delta n_{SC}/\Delta n_{OC}$ analytically with different L_{amb} and with the CTL mobility as a parameter. In addition, numerical simulations are performed as shown in Fig. 7(a). Figure 7(b) shows the term $1 - [\Delta n_{SC}/\Delta n_{OC}]$ as a function of L_{amb} and μ_{CTL} in a 2D color plot, and in Fig. 7(c), we plot the normalized J_{SC} obtained using either ASA or Eq. (14), which illustrates the left- and right-hand sides of Eq. (25). The key conclusion from Fig. 7 is that Eq. (24) indeed works (also when using the numerical simulation) and leads to a perfect correlation between $1 - [\Delta n_{SC}/\Delta n_{OC}]$ and $J_{SC}/J_{SC,max}$, both of which depend on L_{amb} and μ_{CTL} in the same way. Given that $1 - [\Delta n_{SC}/\Delta n_{OC}]$ is experimentally accessible via PL [cf. Eq. (20)], we now have a method to quantify recombination losses due to low mobilities in either the transport or absorber layer.

Quantifying recombination losses at short circuit, or more generally at any voltage that is not the open-circuit voltage, is usually difficult. While J_{SC} is quite easy to measure, $J_{SC,max}$ can only typically be estimated from optical simulations that are based on the complex refractive index of all layers within the cell stack that are difficult to accurately determine. Furthermore, light scattering at the interfaces is often neglected in simulations but can happen in reality. Voltage-dependent PL has a huge advantage, as it is directly proportional to the carrier densities as a function of voltage, which cause recombination. As we have recently shown, from voltage-dependent PL data, the collected J_{SC}, and the ideality factor n_{id}, we can quantify the losses in J_{SC} due to recombination via [102]

$$J_{rec} = \frac{J_{SC}\ \Phi^{1/n_{id}}(V)}{\Phi_{OC}^{1/n_{id}} - \Phi_{SC}^{1/n_{id}}}, \qquad (26)$$

which is an extension of Eq. (23) from short circuit to any arbitrary voltage. Furthermore, Eq. (26) allows J_{rec} to be expressed as a function of J_{SC} and does not contain the *a priori* unknown $J_{SC,max}$.

To investigate losses in the collected J_{SC} due to the mobility of charge carriers in the ETLs {which can be obtained using the space-charge-limited current measurement [e.g., $\mu_{ETL} = 4 \times 10^{-4}$ cm^2/Vs in PCBM (90 nm) and 3×10^{-4} cm^2/Vs in CMC (95 nm)] [101]}, we measure the voltage-dependent photoluminescence on three PSCs with the layer stack glass/ITO/Me-4PACz/Cs$_{0.05}$(FA$_{0.83}$MA$_{0.17}$)$_{0.95}$Pb(I$_{0.83}$Br$_{0.17}$)$_3$/(C$_{60}$, PCBM, or CMC)/BCP/Ag under illumination (around 1 sun). We quantify the quasi-Fermi-level splitting from the PL(V) data as a function of the external bias, as shown in Fig. 8(a). A substantial quasi-Fermi-level splitting at low forward bias is obtained for the PSC with PCBM. Thus, a substantial carrier density is anticipated to remain in the device as a result of the slow extraction in PCBM
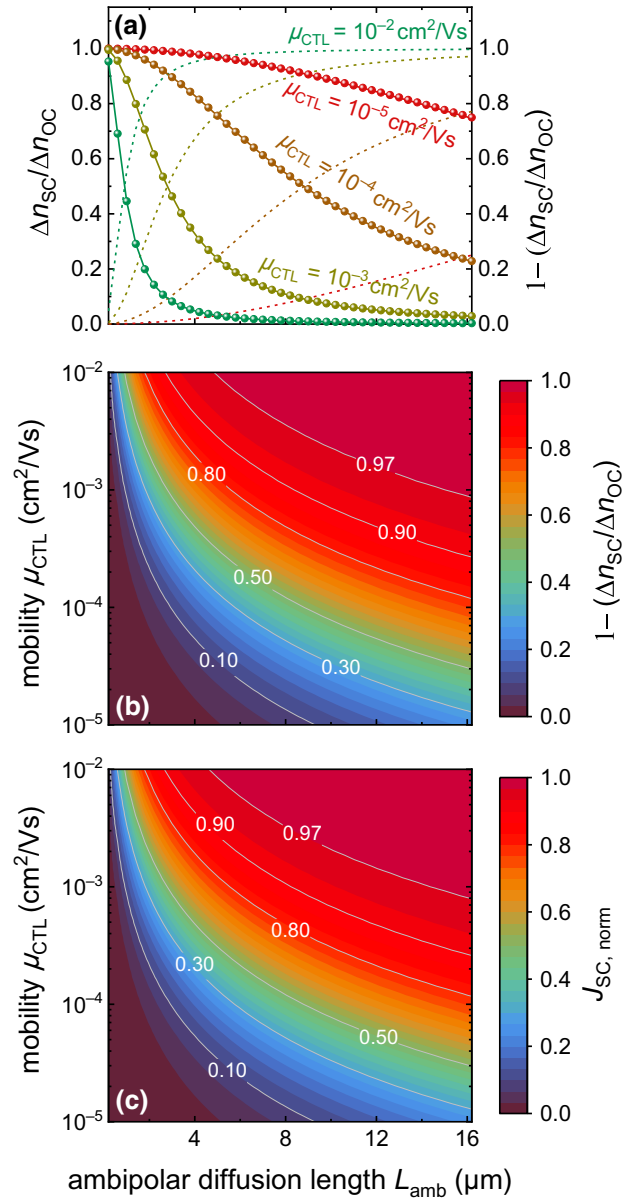

FIG. 7. (a) Excess carrier density at short circuit to open circuit ($\Delta n_{SC}/\Delta n_{OC}$) obtained by numerical simulation by ASA (symbols) and analytical calculations (solid lines), and simulated data of $1 - [\Delta n_{SC}/\Delta n_{OC}]$ (dashed lines). (b) 2D color plot of the difference in carrier density at open and short circuit normalized to their density at open circuit simulated using ASA. (c) 2D color plot of the normalized short-circuit current density, $J_{SC,norm}$. All the data are simulated for a varied range of L_{amb} [$\mu = 35$ cm^2/Vs, $\tau_n + \tau_p$ varies from 10^{-9} to 10^{-5} s] and different μ_{CTLs}. Analytical evaluation corresponding to (b),(c) can be found in the Supplemental Material, Fig. S7 [77].

compared to that in C$_{60}$ and CMC. Thus, the recombination losses at J_{SC} are higher in the samples with PCBM, as shown in Fig. 8(b) (see Figs. S12 and S13 within the Supplemental Material [77]). In CMC, the uncollected carrier density is somewhat lower at short circuit, but it is

strongly voltage dependent, leading to lower fill factors in the finished cells, as seen in Fig. 8(c) (see Fig. S8 and Sec. 2 within the Supplemental Material [77]). While the differences in behavior between the different ETLs can be quantified using PL, identifying their precise origin is beyond the scope of the paper. We assume that the differences between the three fullerenes are related to differences in electron mobility and in band alignment at the perovskite-ETL interface [101].

V. CONCLUSION

The diffusion length, L_{amb}, of halide perovskite absorbers for photovoltaics is an appealing property that is frequently mentioned as a synonym for good electronic properties. Furthermore, it is often implicitly assumed to be a necessary and possibly also sufficient condition for efficient charge collection. The rationale behind this statement originates from the logic of p-n junction solar cells and from the assumption of perfect collection at the edge of the space-charge region in a p-n junction solar cell. In halide perovskites, a perfectly collecting boundary condition is hardly a realistic scenario, given the abundance of various organic contact layers that are often, but not always, intrinsic and that feature electron and hole mobilities which are typically much lower than that of the perovskite. The physics of charge-carrier collection in perovskite solar cells is therefore different from that of many other photovoltaic technologies. A sufficiently long diffusion length remains a necessary condition for efficient charge collection, but it is by no means a sufficient criterion. In fact, it is likely the less important of two key criteria, namely, $L_{amb} \gg d$ and $S_{CTL}(\tau_n + \tau_p) \gg d$. It is this latter criterion that is key to understanding efficient collection in perovskite solar cells and that is currently not discussed in the literature. While the contact layers are understood to be a potential cause for ohmic losses and reduced fill factors, intrinsic or lowly doped contact layers can also have a direct impact on the short-circuit current without necessarily affecting the fill factor. This is due to their ability to modulate the carrier density at short circuit or low forward bias inside the absorber layer. The lower, e.g., mobility inside ETL or HTL, the higher the carrier density and the higher the recombination rate at a given charge-carrier lifetime. Thus, the value of the diffusion length inside the absorber depends on the charge-carrier density inside the absorber, and this latter quantity depends on the conductivity of undoped contact layers. While being present to some degree in any photovoltaic technology [55,84], this effect is particularly strong in halide perovskites, as they have thin absorber layers with quite decent mobilities and long lifetimes that are then interfaced with (often) low-mobility transport layers. In addition to highlighting the role of the condition $S_{CTL}(\tau_n + \tau_p) \gg d$ for efficient collection, we also
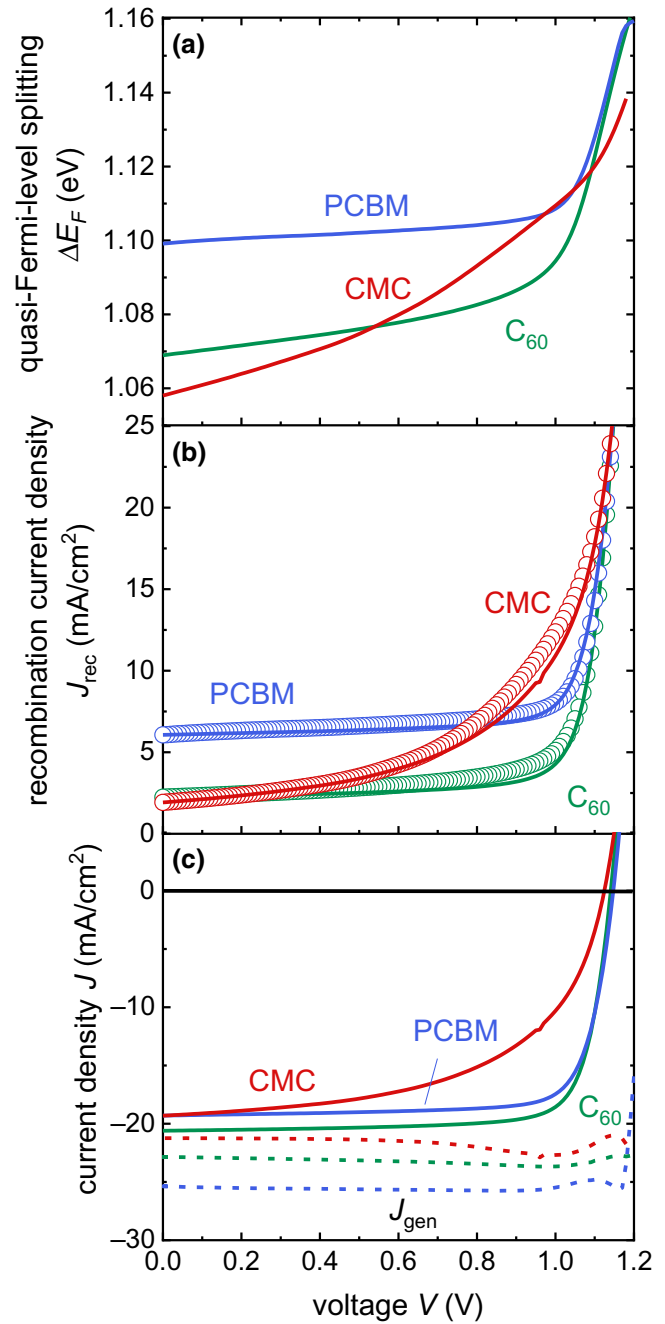

FIG. 8. (a) Quasi-Fermi-level splitting determined from voltage-dependent PL measurements as a function of externally applied bias for PSCs of different ETLs (C_{60}, PCBM, and CMC). (b) Recombination current density calculated from PL data (symbols) according to Eq. (26); solid lines represent the recombination current obtained from the measured J-V curves plus the maximum photocurrent for the three PSCs of different ETLs. (c) Current-voltage curves measured by the PL(V) imaging setup under illumination at around 1 sun; voltage sweeps for the J-V curves are measured in the reverse direction; dashed lines show the maximum photocurrent corresponds to each sample. (See Fig. S8 within the Supplemental Material [77] for the up-sweeping measurement.)

illustrate the importance of voltage-dependent photoluminescence measurements. These measurements are able to identify and quantify recombination losses that are caused by inefficient charge collection and inefficient transport through the ETL or HTL. In particular, they allow identifying situations where the loss is mainly at short circuit and the shape of the current-voltage curve does not indicate a significant fill-factor loss.

APPENDIX A: METHODS

1. Materials

Formamidinium iodide (FAI) and methylammonium bromide (MABr) are purchased from Greatcell Solar. Lead iodide (PbI_2) and lead bromide ($PbBr_2$) are purchased from Tokyo Chemical Industry (TCI) and Acros Organics, respectively. Cesium iodide (CsI) is purchased from Sigma Aldrich. [4-(3,6-Dimethyl-9*H*-carbazol-9-yl)butyl]phosphonic acid (Me-4PACz) is purchased from TCI. Bathocuproine (BCP, >99.0%) and C_{60}-fused *N*-methylpyrrolidine-*m*-C12-phenyl (CMC) are purchased from TCI. [6,6]-Phenyl-C61-butyric acid methyl ester (PCBM) is purchased from Solenne (Netherlands). Anhydrous ethanol (EtOH), *N*,*N*-dimethylformamide (DMF, 99.8%), dimethyl sulfoxide (DMSO), *N*-methyl-2-pyrrolidone (NMP), and chlorobenzene (99.8%) are purchased from Sigma-Aldrich and used as received.

2. Device fabrication

The prepatterned ITO substrates (2.0×2.0 cm^2) are bought from Kintec and ultrasonically cleaned with Hellmanex soap solution (2% in deionized water), deionized water, acetone, and 2-propanol for 10 min each. Before being transferred to the N_2-filled glove box, as-cleaned ITO substrates are treated with oxygen plasma (Diener Zepto, 50 W) for 15 min. Me-4PACz solution (0.3 mg/mL) in EtOH is spin-coated onto the ITO substrates at 3000 revolutions per minute (rpm) for 30 s [with a ramping rate of 500 rpm s^{-1}] followed by thermally annealing at 100 °C for 10 min. Triple-cation perovskite precursor solution in DMF : DMSO : NMP (4 : 0.7 : 0.3 v/v/v ratio) is prepared by mixing PbI_2 (1.54 *M*) and $PbBr_2$ (1.5 *M*) with FAI (1.5 *M*) and MABr (1.5 *M*), respectively, and stirred overnight at 70 °C followed by adding 5% 1.5-*M* CsI solution in DMSO to the aforementioned FAMA-based perovskite solution to form the triple-cation perovskite solution. Before spin-coating the solution (120 µl/substrate)

at 3500 rpm for 35 s (500 rpm s^{-1}) the perovskite solution is filtered using 0.45-µm polytetrafluoroethylene filter. During spin-coating, 300 µl chlorobenzene is used as the antisolvent 15 s before the end of the spin-coating step followed by annealing the perovskite film at 100 °C for 40 min to form a high-quality perovskite thin film. After cooling the substrates to room temperature, a PCBM (20 mg/mL) [or CMC (10 mg/mL)] solution in chlorobenzene (60 µl/substrate) is spin-coated on top of the perovskite layer at a speed of 1200 rpm for 60 s (with a ramping rate of 400 rpm s^{-1}). A C_{60} (25 nm) layer is deposited by thermal evaporation in a K. J. Lesker Mini Spectros System attached to the glove box ($<5 \times 10^{-6}$ Pa) at a rate of 0.2 Å/s. Finally, BCP (8 nm) and Ag (80 nm) are thermally evaporated on all the ETL/perovskite/Me-4PACz device stacks sequentially using the aforementioned evaporator setup.

3. Device characterization

a. Current density-voltage (*J*-*V*) characterization

The *J*-*V* curves are measured on a calibrated AM1.5 spectrum of a class AAA solar simulator (WACOM-WXS-140S-Super-L2 with a combined xenon-halogen lamp-based system). In addition to the *J*-*V* curves, the J_{SC}/V_{OC} measurements at different light intensities are measured using a light-emitting diode (LED) solar simulator, which is directly integrated into the glove box. The LED solar simulation is equipped with a white-light LED (Cree XLamp CXA3050). The illuminance of the LED solar simulator is adjusted to 1 sun conditions using the short-circuit current density (J_{SC}) resulting from the external quantum efficiency (EQE) measurement of a perovskite cell. Each 2.0×2.0-cm^2 substrate contains four solar cells with an active area of 0.16 cm^2 each and the device *J*-*V* is measured with a 3.0×3.0-mm^2 shadow mask, and J_{SC}/V_{OC} characteristics are measured without any shadow mask.

b. Intensity-dependent transient photoluminescence (TRPL)

The transient photoluminescence is measured for passivated and nonpassivated thin films of the perovskite material on glass and for a perovskite solar cell with layer stacks [glass/ITO/Me-4PACz/$Cs_{0.05}(FA_{0.83}MA_{0.17})_{0.95}Pb(I_{0.83}Br_{0.17})_3$/$C_{60}$/BCP/Ag] using time-correlated single-photon-counting technique. A laser of 638-nm wavelength, 25.56-µm spot size, and 100 kHz is used to excite the samples. The measurements are done using different laser intensities [different optical density (OD) filters (e.g., 2.3 OD, 1.6 OD, 0.6 OD, . . ., 0 OD)] for 300 s. To get information about whether the samples are intrinsic, the intensity-dependent TRPL decays are analyzed at $t = 0$ following the method of Peña-Camargo *et al.* [93].

c. EQE

The EQE of perovskite devices with different ETLs are measured using a xenon light source (Osram XPO150W) and a Bentham monochromator (TMC300) with a spectral range between 300 and 1100 nm. The light source is calibrated with a calibrated silicon photodiode (Gigahertz-Optik SSO-PD100-04) as a reference. The chopper frequency is set to 72 Hz; the three devices are measured with a spectral range between 300 and 850 nm with a step size of 10 nm. For measurements, the devices are sealed, in a nitrogen-filled glove box, in a measurement box with a quartz glass window to avoid exposure to the external ambient atmosphere.

d. Voltage-dependent photoluminescence measurement (imaging technique)

The PL intensity is measured along the J-V curve using a self-made setup consisting of a detection CCD camera with a cooling system, a power supply, a Keithley 2400 source measure unit, and a bias light source. The perovskite solar cells with different electron-transport layers (C_{60}, PCBM, and CMC) are excited (3.0×3.0 mm^2) electrically and optically using a set of five green LEDs ($\lambda = 540$ nm) with homogeneous illumination at a fluence of about 1 sun. The PL intensity is captured by a CCD camera from Andor supplied with an objective lens and incorporates sensors that have 1024×1024 pixels. The background is measured first and a flat-field correction is done to obtain the corrected images in the end. The J-V curves are measured in both forward and reverse directions with a voltage step of 0.01 V, and data acquisition is accomplished with an exposure time of 1 s with five accumulations for each voltage step.

---

[1] T. C. Sum and N. Mathews, Advancements in perovskite solar cells: Photophysics behind the photovoltaics, Energy Environ. Sci. **7**, 2518 (2014).

[2] Q. Dong, Y. Fang, Y. Shao, P. Mulligan, J. Qiu, L. Cao, and J. Huang, Electron-hole diffusion lengths > 175 mm in solution-grown $CH_3NH_3PbI_3$ single crystals, Science **347**, 967 (2015).

[3] G. Xing, N. Mathews, S. Sun, S. S. Lim, Y. M. Lam, M. Grätzel, S. Mhaisalkar, and T. C. Sum, Long-range balanced electron- and hole-transport lengths in organic-inorganic $CH_3NH_3PbI_3$, Science **342**, 344 (2013).

[4] L. M. Herz, Charge-carrier mobilities in metal halide perovskites: Fundamental mechanisms and limits, ACS Energy Lett. **2**, 1539 (2017).

[5] V. M. Le Corre, E. A. Duijnstee, O. El Tambouli, J. M. Ball, H. J. Snaith, J. Lim, and L. J. A. Koster, Revealing charge carrier mobility and defect densities in metal halide perovskites via space-charge-limited current measurements, ACS Energy Lett. **6**, 1087 (2021).

[6] Y. Bi, E. M. Hutter, Y. Fang, Q. Dong, J. Huang, and T. J. Savenije, Charge carrier lifetimes exceeding 15 μs in methylammonium lead iodide single crystals, J. Phys. Chem. Lett. **7**, 923 (2016).

[7] F. Staub, H. Hempel, J.-C. Hebig, J. Mock, U. W. Paetzold, U. Rau, T. Unold, and T. Kirchartz, Beyond Bulk Lifetimes: Insights into Lead Halide Perovskite Films from Time-Resolved Photoluminescence, Phys. Rev. Appl. **6**, 044017 (2016).

[8] S. D. Stranks, V. M. Burlakov, T. Leijtens, J. M. Ball, A. Goriely, and H. J. Snaith, Recombination Kinetics in Organic-Inorganic Perovskites: Excitons, Free Charge, and Subgap States, Phys. Rev. Appl. **2**, 034007 (2014).

[9] G. Hodes and P. V. Kamat, Understanding the implication of carrier diffusion length in photovoltaic cells, J. Phys. Chem. Lett. **6**, 4090 (2015).

[10] I. Levine, S. Gupta, A. Bera, D. Ceratti, G. Hodes, D. Cahen, D. Guo, T. J. Savenije, J. Ávila, H. J. Bolink, *et al.*, Can we use time-resolved measurements to get steady-state transport data for halide perovskites?, J. Appl. Phys. **124**, 103103 (2018).

[11] C. Wehrenfennig, G. E. Eperon, M. B. Johnston, H. J. Snaith, and L. M. Herz, High charge carrier mobilities and lifetimes in organolead trihalide perovskites, Adv. Mater. **26**, 1584 (2014).

[12] S. D. Stranks, G. E. Eperon, G. Grancini, C. Menelaou, M. J. P. Alcocer, T. Leijtens, L. M. Herz, A. Petrozza, and H. J. Snaith, Electron-hole diffusion lengths exceeding 1 micrometer in an organometal trihalide perovskite absorber, Science **342**, 341 (2013).

[13] F. Zhang, B. Yang, Y. Li, W. Deng, and R. He, Extra long electron–hole diffusion lengths in $CH_3NH_3PbI_{3-x}Cl_x$ perovskite single crystals, J. Mater. Chem. C **5**, 8431 (2017).

[14] A. Kitai, *Principles of Solar Cells, LEDs and Related Devices: The Role of the PN Junction* (Wiley, United Kingdom, 2018).

[15] R. Brendel, *Thin-Film Crystalline Silicon Solar Cells: Physics and Technology* (Wiley, Weinheim, 2011).

[16] D. A. Neamen, *Semiconductor Physics and Devices: Basic Principles* (McGraw-Hill, New York, 2012).

[17] E. Edri, S. Kirmayer, S. Mukhopadhyay, K. Gartsman, G. Hodes, and D. Cahen, Elucidating the charge carrier separation and working mechanism of $CH_3NH_3PbI_{3-x}Cl_x$ perovskite solar cells, Nat. Commun. **5**, 3461 (2014).

[18] J. You, Z. Hong, Y. Yang, Q. Chen, M. Cai, T.-B. Song, C.-C. Chen, S. Lu, Y. Liu, H. Zhou, *et al.*, Low-temperature solution-processed perovskite solar cells with high efficiency and flexibility, ACS Nano **8**, 1674 (2014).

[19] T. Kirchartz, W. Gong, S. A. Hawks, T. Agostinelli, R. C. I. MacKenzie, Y. Yang, and J. Nelson, Sensitivity of the Mott–Schottky analysis in organic solar cells, J. Phys. Chem. C **116**, 7672 (2012).

[20] N. Tessler and Y. Vaynzof, Insights from device modeling of perovskite solar cells, ACS Energy Lett. **5**, 1260 (2020).

[21] P. Calado, A. M. Telford, D. Bryant, X. Li, J. Nelson, B. C. O'Regan, and P. R. F. Barnes, Evidence for ion migration in hybrid perovskite solar cells with minimal hysteresis, Nat. Commun. **7**, 13831 (2016).

[22] J. Thiesbrummel, V. M. Le Corre, F. Peña-Camargo, L. Perdigón-Toro, F. Lang, F. Yang, M. Grischek, E.

Gutierrez-Partida, J. Warby, M. D. Farrar, *et al.*, Universal current losses in perovskite solar cells due to mobile ions, Adv. Energy Mater. **11**, 2101447 (2021).

[23] V. M. Le Corre, J. Diekmann, F. Peña-Camargo, J. Thiesbrummel, N. Tokmoldin, E. Gutierrez-Partida, K. P. Peters, L. Perdigón-Toro, M. H. Futscher, F. Lang, *et al.*, Quantification of efficiency losses due to mobile ions in perovskite solar cells via fast hysteresis measurements, Solar RRL **6**, 2100772 (2022).

[24] P. Würfel and U. Würfel, *Physics of solar cells: From basic principles to advanced concepts*, 3rd ed. (Wiley-VCH Verlag GmbH & Co. KGaA, Weinheim, 2016).

[25] J. Bisquert, D. Cahen, G. Hodes, S. Rühle, and A. Zaban, Physical chemical principles of photovoltaic conversion with nanoparticulate, mesoporous dye-sensitized solar cells, J. Phys. Chem. B **108**, 8106 (2004).

[26] C. Zuo, H. J. Bolink, H. Han, J. Huang, D. Cahen, and L. Ding, Advances in perovskite solar cells, Adv. Sci. **3**, 1500324 (2016).

[27] Y. Wu, D. Yan, J. Peng, T. Duong, Y. Wan, S. P. Phang, H. Shen, N. Wu, C. Barugkin, X. Fu, *et al.*, Monolithic perovskite/silicon-homojunction tandem solar cell with over 22% efficiency, Energy Environ. Sci. **10**, 2472 (2017).

[28] Y. Rong, Y. Hu, A. Mei, H. Tan, M. I. Saidaminov, S. I. Seok, M. D. McGehee, E. H. Sargent, and H. Han, Challenges for commercializing perovskite solar cells, Science **361**, eaat8235 (2018).

[29] N. R. Paudel and Y. Yan, Application of copper thiocyanate for high open-circuit voltages of CdTe solar cells, Prog. Photovoltaics **24**, 94 (2016).

[30] O. Magen and N. Tessler, Charge blocking layers in thin-film/amorphous photovoltaics, J. Appl. Phys. **120**, 194502 (2016).

[31] T. Kim, J. Lim, and S. Song, Recent progress and challenges of electron transport layers in organic–inorganic perovskite solar cells, Energies **13**, 5572 (2020).

[32] V. M. Le Corre, M. Stolterfoht, L. Perdigón Toro, M. Feuerstein, C. Wolff, L. Gil-Escrig, H. J. Bolink, D. Neher, and L. J. A. Koster, Charge transport layers limiting the efficiency of perovskite solar cells: How to optimize conductivity, doping, and thickness, ACS Appl. Energy Mater. **2**, 6280 (2019).

[33] S. Bitton and N. Tessler, Electron/hole blocking layers as ionic blocking layers in perovskite solar cells, J. Mater. Chem. C **9**, 1888 (2021).

[34] U. Rau and T. Kirchartz, Charge carrier collection and contact selectivity in solar cells, Adv. Mater. Interfaces **6**, 1900252 (2019).

[35] K. E. Egelhofer Ruegger, E. T. Roe, and M. C. Lonergan, Solar cell contacts: Quantifying the impact of interfacial layers on selectivity, recombination, charge transfer, and V_{oc}, Sustainable Energy Fuels **5**, 1767 (2021).

[36] W. Ke, G. Fang, J. Wan, H. Tao, Q. Liu, L. Xiong, P. Qin, J. Wang, H. Lei, G. Yang, *et al.*, Efficient hole-blocking layer-free planar halide perovskite thin-film solar cells, Nat. Commun. **6**, 6700 (2015).

[37] O. Malinkiewicz, A. Yella, Y. H. Lee, G. M. Espallargas, M. Graetzel, M. K. Nazeeruddin, and H. J. Bolink, Perovskite solar cells employing organic charge-transport layers, Nat. Photonics **8**, 128 (2014).

[38] T. Kirchartz, J. Bisquert, I. Mora-Sero, and G. Garcia-Belmonte, Classification of solar cells according to mechanisms of charge separation and charge collection, Phys. Chem. Chem. Phys. **17**, 4007 (2015).

[39] B. Dänekamp, N. Droseros, D. Tsokkou, V. Brehm, P. P. Boix, M. Sessolo, N. Banerji, and H. J. Bolink, Influence of hole transport material ionization energy on the performance of perovskite solar cells, J. Mater. Chem. C **7**, 523 (2019).

[40] T. Kirchartz, L. Krückemeier, and E. L. Unger, Research update: Recombination and open-circuit voltage in lead-halide perovskites, APL Mater. **6**, 100702 (2018).

[41] T. Kirchartz, J. A. Márquez, M. Stolterfoht, and T. Unold, Photoluminescence-based characterization of halide perovskites for photovoltaics, Adv. Energy Mater. **10**, 1904134 (2020).

[42] Z. Liu, L. Krückemeier, B. Krogmeier, B. Klingebiel, J. A. Márquez, S. Levcenko, S. Öz, S. Mathur, U. Rau, T. Unold, *et al.*, Open-circuit voltages exceeding 1.26 V in planar methylammonium lead iodide perovskite solar cells, ACS Energy Lett. **4**, 110 (2019).

[43] D. Bi, L. Yang, G. Boschloo, A. Hagfeldt, and E. M. J. Johansson, Effect of different hole transport materials on recombination in $CH_3NH_3PbI_3$ perovskite-sensitized mesoscopic solar cells, J. Phys. Chem. Lett. **4**, 1532 (2013).

[44] L. Krückemeier, U. Rau, M. Stolterfoht, and T. Kirchartz, How to report record open-circuit voltages in lead-halide perovskite solar cells, Adv. Energy Mater. **10**, 1902573 (2020).

[45] Z. Guo, A. K. Jena, G. M. Kim, and T. Miyasaka, The high open-circuit voltage of perovskite solar cells: A review, Energy Environ. Sci. **15**, 3171 (2022).

[46] J. A. Nelson, *The Physics of Solar Cells* (World Scientific Publishing Company, London, 2003).

[47] K. W. Böer, *Handbook of the Physics of Thin-Film Solar Cells* (Springer, Berlin Heidelberg, 2014).

[48] A. Kitai, *Principles of Solar Cells, LEDs and Diodes: The role of the PN junction* (Wiley, United Kingdom, 2011).

[49] T. Kirchartz, *Generalized detailed balance theory of solar cells* (Forschungszentrum Jülich, Germany, 2009), Vol. 38.

[50] C. Hu, *Modern Semiconductor Devices for Integrated Circuits* (Prentice Hall, United States, 2010).

[51] K. Yoshikawa, H. Kawasaki, W. Yoshida, T. Irie, K. Konishi, K. Nakano, T. Uto, D. Adachi, M. Kanematsu, H. Uzu, *et al.*, Silicon heterojunction solar cell with interdigitated back contacts for a photoconversion efficiency over 26%, Nat. Energy **2**, 17032 (2017).

[52] T. G. Allen, J. Bullock, X. Yang, A. Javey, and S. De Wolf, Passivating contacts for crystalline silicon solar cells, Nat. Energy **4**, 914 (2019).

[53] A. Richter, R. Müller, J. Benick, F. Feldmann, B. Steinhauser, C. Reichel, A. Fell, M. Bivour, M. Hermle, and S. W. Glunz, Design rules for high-efficiency both-sides-contacted silicon solar cells with balanced charge carrier transport and recombination losses, Nat. Energy **6**, 429 (2021).

[54] M. Köhler, M. Pomaska, P. Procel, R. Santbergen, A. Zamchiy, B. Macco, A. Lambertz, W. Duan, P. Cao, B. Klingebiel, *et al.*, A silicon carbide-based highly

transparent passivating contact for crystalline silicon solar cells approaching efficiencies of 24%, Nat. Energy **6**, 529 (2021).

[55] K. Misiakos and F. A. Lindholm, Minority-carrier accumulation at the base edge of a junction space-charge region under short-circuit conditions, Solid-State Electron. **30**, 755 (1987).

[56] C. Donolato, A reciprocity theorem for charge collection, Appl. Phys. Lett. **46**, 270 (1985).

[57] M. A. Green, Generalized relationship between dark carrier distribution and photocarrier collection in solar cells, J. Appl. Phys. **81**, 268 (1997).

[58] K. Misiakos and F. A. Lindholm, Generalized reciprocity theorem for semiconductor devices, J. Appl. Phys. **58**, 4743 (1985).

[59] B. E. Pieters, J. Krč, and M. Zeman, in *2006 IEEE 4th World Conference on Photovoltaic Energy Conference* (2006), Vol. 2, pp. 1513.

[60] A. M. A. Leguy, P. Azarhoosh, M. I. Alonso, M. Campoy-Quiles, O. J. Weber, J. Yao, D. Bryant, M. T. Weller, J. Nelson, A. Walsh, *et al.*, Experimental and theoretical optical properties of methylammonium lead halide perovskites, Nanoscale **8**, 6317 (2016).

[61] S. De Wolf, J. Holovsky, S.-J. Moon, P. Löper, B. Niesen, M. Ledinsky, F.-J. Haug, J.-H. Yum, and C. Ballif, Organometallic halide perovskites: Sharp optical absorption edge and its relation to photovoltaic performance, J. Phys. Chem. Lett. **5**, 1035 (2014).

[62] J. Jiang, X. Sun, X. Chen, B. Wang, Z. Chen, Y. Hu, Y. Guo, L. Zhang, Y. Ma, L. Gao, *et al.*, Carrier lifetime enhancement in halide perovskite via remote epitaxy, Nat. Commun. **10**, 4145 (2019).

[63] Q. Jiang, Y. Zhao, X. Zhang, X. Yang, Y. Chen, Z. Chu, Q. Ye, X. Li, Z. Yin, and J. You, Surface passivation of perovskite film for efficient solar cells, Nat. Photonics **13**, 460 (2019).

[64] X. Zheng, Y. Hou, C. Bao, J. Yin, F. Yuan, Z. Huang, K. Song, J. Liu, J. Troughton, N. Gasparini, *et al.*, Managing grains and interfaces via ligand anchoring enables 22.3%-efficiency inverted perovskite solar cells, Nat. Energy **5**, 131 (2020).

[65] L. Krückemeier, B. Krogmeier, Z. Liu, U. Rau, and T. Kirchartz, Understanding transient photoluminescence in halide perovskite layer stacks and solar cells, Adv. Energy Mater. **11**, 2003489 (2021).

[66] Q. Han, S.-H. Bae, P. Sun, Y.-T. Hsieh, Y. Yang, Y. S. Rim, H. Zhao, Q. Chen, W. Shi, G. Li, *et al.*, Single crystal formamidinium lead iodide (FAPbI$_3$): Insight into the structural, optical, and electrical properties, Adv. Mater. **28**, 2253 (2016).

[67] U. Würfel, A. Cuevas, and P. Würfel, Charge carrier separation in solar cells, IEEE J. Photovoltaics **5**, 461 (2015).

[68] I. M. Hermes, Y. Hou, V. W. Bergmann, C. J. Brabec, and S. A. L. Weber, The interplay of contact layers: How the electron transport layer influences interfacial recombination and hole extraction in perovskite solar cells, J. Phys. Chem. Lett. **9**, 6249 (2018).

[69] S. Li, Y.-L. Cao, W.-H. Li, and Z.-S. Bo, A brief review of hole transporting materials commonly used in perovskite solar cells, Rare Met. **40**, 2712 (2021).

[70] L. Lin, T. W. Jones, T. C.-J. Yang, N. W. Duffy, J. Li, L. Zhao, B. Chi, X. Wang, and G. J. Wilson, Inorganic electron transport materials in perovskite solar cells, Adv. Funct. Mater. **31**, 2008300 (2021).

[71] D. Zhou, T. Zhou, Y. Tian, X. Zhu, and Y. Tu, Perovskite-based solar cells: Materials, methods, and future perspectives, J. Nanomater. **2018**, 8148072 (2018).

[72] P. Kaienburg, L. Krückemeier, D. Lübke, J. Nelson, U. Rau, and T. Kirchartz, How solar cell efficiency is governed by the $\alpha\mu\tau$ product, Phys. Rev. Res. **2**, 023109 (2020).

[73] B. Roose, Q. Wang, and A. Abate, The role of charge selective contacts in perovskite solar cell stability, Adv. Energy Mater. **9**, 1803140 (2019).

[74] M. Stolterfoht, C. M. Wolff, J. A. Márquez, S. Zhang, C. J. Hages, D. Rothhardt, S. Albrecht, P. L. Burn, P. Meredith, T. Unold, *et al.*, Visualization and suppression of interfacial recombination for high-efficiency large-area pin perovskite solar cells, Nat. Energy **3**, 847 (2018).

[75] C. Motta, F. El-Mellouhi, and S. Sanvito, Charge carrier mobility in hybrid halide perovskites, Sci. Rep. **5**, 12746 (2015).

[76] J. Siekmann, S. Ravishankar, and T. Kirchartz, Apparent defect densities in halide perovskite thin films and single crystals, ACS Energy Lett. **6**, 3244 (2021).

[77] See the Supplemental Material at http://link.aps.org/supplemental/10.1103/PRXEnergy.2.013004 for simulation parameters, simulations related to the impact of mobility in the charge-transport layer on the device performance, and simulations to aid analytical evaluation and experimental determination of the collected photocurrent versus J_{SC}. A discussion of quantifying recombination losses due to the mobility in PSCs by using the voltage-dependent photoluminescence experiment. References [41,74–76,93,102] are included in the Supplemental Material.

[78] O. J. Sandberg, J. Kurpiers, M. Stolterfoht, D. Neher, P. Meredith, S. Shoaee, and A. Armin, On the question of the need for a built-in potential in perovskite solar cells, Adv. Mater. Interfaces **7**, 2000041 (2020).

[79] B. Das, Z. Liu, I. Aguilera, U. Rau, and T. Kirchartz, Defect tolerant device geometries for lead-halide perovskites, Mater. Adv. **2**, 3655 (2021).

[80] D. Hinken, K. Bothe, K. Ramspeck, S. Herlufsen, and R. Brendel, Determination of the effective diffusion length of silicon solar cells from photoluminescence, J. Appl. Phys. **105**, 104516 (2009).

[81] O. Breitenstein, An alternative one-diode model for illuminated solar cells, IEEE J. Photovoltaics **4**, 899 (2014).

[82] S. Robinson, A. Aberle, and M. Green, Departures from the principle of superposition in silicon solar cells, J. Appl. Phys. **76**, 7920 (1994).

[83] F. A. Lindholm, J. G. Fossum, and E. L. Burgess, Application of the superposition principle to solar-cell analysis, IEEE Trans. Electron Devices **26**, 165 (1979).

[84] U. Rau, V. Huhn, and B. E. Pieters, Luminescence Analysis of Charge-Carrier Separation and Internal Series-Resistance Losses in Cu(In, Ga)Se$_2$ Solar Cells, Phys. Rev. Appl. **14**, 014046 (2020).

[85] U. Würfel, D. Neher, A. Spies, and S. Albrecht, Impact of charge transport on current–voltage characteristics and power-conversion efficiency of organic solar cells, Nat. Commun. **6**, 6951 (2015).

[86] T. C. M. Müller, B. E. Pieters, U. Rau, and T. Kirchartz, Analysis of the series resistance in pin-type thin-film silicon solar cells, J. Appl. Phys. **113**, 134503 (2013).

[87] V. Sarritzu, N. Sestu, D. Marongiu, X. Chang, S. Masi, A. Rizzo, S. Colella, F. Quochi, M. Saba, A. Mura, *et al.*, Optical determination of Shockley-Read-Hall and interface recombination currents in hybrid perovskites, Sci. Rep. **7**, 44629 (2017).

[88] M. Stolterfoht, P. Caprioglio, C. M. Wolff, J. A. Márquez, J. Nordmann, S. Zhang, D. Rothhardt, U. Hörmann, Y. Amir, A. Redinger, *et al.*, The impact of energy alignment and interfacial recombination on the internal and external open-circuit voltage of perovskite solar cells, Energy Environ. Sci. **12**, 2778 (2019).

[89] L. Krückemeier, Z. Liu, B. Krogmeier, U. Rau, and T. Kirchartz, Consistent interpretation of electrical and optical transients in halide perovskite layers and solar cells, Adv. Energy Mater. **11**, 2102290 (2021).

[90] T. Du, W. Xu, S. Xu, S. R. Ratnasingham, C.-T. Lin, J. Kim, J. Briscoe, M. A. McLachlan, and J. R. Durrant, Light-intensity and thickness dependent efficiency of planar perovskite solar cells: Charge recombination versus extraction, J. Mater. Chem. C **8**, 12648 (2020).

[91] M. Stolterfoht, V. M. Le Corre, M. Feuerstein, P. Caprioglio, L. J. A. Koster, and D. Neher, Voltage-dependent photoluminescence and how it correlates with the fill factor and open-circuit voltage in perovskite solar cells, ACS Energy Lett. **4**, 2887 (2019).

[92] K. Tvingstedt, O. Malinkiewicz, A. Baumann, C. Deibel, H. J. Snaith, V. Dyakonov, and H. J. Bolink, Radiative efficiency of lead iodide based perovskite solar cells, Sci. Rep. **4**, 6071 (2014).

[93] F. Peña-Camargo, J. Thiesbrummel, H. Hempel, A. Musiienko, V. M. L. Corre, J. Diekmann, J. Warby, T. Unold, F. Lang, D. Neher, *et al.*, Revealing the doping density in perovskite solar cells and its impact on device performance, Appl. Phys. Rev. **9**, 021409 (2022).

[94] T. Trupke, R. A. Bardos, M. D. Abbott, and J. E. Cotter, Suns-photoluminescence: Contactless determination of current-voltage characteristics of silicon wafers, Appl. Phys. Lett. **87**, 093503 (2005).

[95] L. Wagner, P. Schygulla, J. P. Herterich, M. Elshamy, D. Bogachuk, S. Zouhair, S. Mastroianni, U. Würfel, Y. Liu, and S. M. Zakeeruddin, Revealing fundamentals of charge extraction in photovoltaic devices through potentiostatic photoluminescence imaging, Matter **5**, 2352 (2022).

[96] J. Herterich, C. Baretzky, M. Unmüssig, C. Maheu, N. Glissmann, J. Gutekunst, G. Loukeris, T. Mayer, M. Kohlstädt, J. P. Hofmann, *et al.*, Toward understanding the short-circuit current loss in perovskite solar cells with 2D passivation layers, Solar RRL **6**, 2200195 (2022).

[97] V. Campanari, F. Martelli, A. Agresti, S. Pescetelli, N. Y. Nia, F. Di Giacomo, D. Catone, P. O'Keeffe, S. Turchini, B. Yang, *et al.*, Reevaluation of photoluminescence intensity as an indicator of efficiency in perovskite solar cells, Solar RRL **6**, 2200049 (2022).

[98] A. Dasgupta, S. Mahesh, P. Caprioglio, Y.-H. Lin, K.-A. Zaininger, R. D. J. Oliver, P. Holzhey, S. Zhou, M. M. McCarthy, J. A. Smith, *et al.*, Visualizing macroscopic inhomogeneities in perovskite solar cells, ACS Energy Lett. **7**, 2311 (2022).

[99] P. Caprioglio, C. M. Wolff, O. J. Sandberg, A. Armin, B. Rech, S. Albrecht, D. Neher, and M. Stolterfoht, On the origin of the ideality factor in perovskite solar cells, Adv. Energy Mater. **10**, 2000502 (2020).

[100] M. Stolterfoht, M. Grischek, P. Caprioglio, C. M. Wolff, E. Gutierrez-Partida, F. Peña-Camargo, D. Rothhardt, S. Zhang, M. Raoufi, J. Wolansky, *et al.*, How to quantify the efficiency potential of neat perovskite films: Perovskite semiconductors with an implied efficiency exceeding 28%, Adv. Mater. **32**, 2000080 (2020).

[101] Z. Liu, J. Siekmann, B. Klingebiel, U. Rau, and T. Kirchartz, Interface optimization via fullerene blends enables open-circuit voltages of 1.35 V in $CH_3NH_3Pb(I_{0.8}Br_{0.2})_3$ solar cells, Adv. Energy Mater. **11**, 2003386 (2021).

[102] D. Grabowski, Z. Liu, G. Schöpe, U. Rau, and T. Kirchartz, Fill factor losses and deviations from the superposition principle in lead halide perovskite solar cells, Solar RRL **6**, 2200507 (2022).